ELSEVIER

International Journal of Heat and Fluid Flow 23 (2002) 547–553

International Journal of HEAT AND FLUID FLOW

www.elsevier.com/locate/ijhff

Direct numerical simulation of a transitional rectangular jet

B. Rembold *, N.A. Adams, L. Kleiser

Institute of Fluid Dynamics, ETH Zürich, ETH Zentrum, CH-8092 Zürich, Switzerland

Abstract

A well-resolved numerical simulation of a Mach 0.5 jet exiting from a rectangular shaped nozzle with an aspect ratio of 5 into a quiescent ambient was performed at a Reynolds number of 2000 based on the narrow side of the nozzle. The transition process was triggered by the most unstable symmetric linear eigenmode of a parallel laminar jet profile at the nozzle exit. We observe a shear-layer roll-up for the laminar jet and subsequently a very rapid transition to small-scale turbulence. The asymmetry of the velocity profile with respect to the jet axis leads to a rapid spreading of the jet along its minor axis within the so-called characteristic region as expected from experimental observations for similar configurations. © 2002 Elsevier Science Inc. All rights reserved.

PACS: 47.27.Cn; 47.27.Wg; 47.27.Eq; 27.20.Ft
Keywords: Jet; Rectangular; Transition to turbulence; DNS

1. Introduction

Due to their significance in practical applications (propulsion, combustion) jet flows have been extensively studied in the past, experimentally as well as numerically. Recently, non-axisymmetric jet configurations found increased attention owing to their superior mixing properties compared with round jets (Gutmark and Grinstein, 1999). Computational studies of these flows are being performed in order to identify means to increase mixing, accelerate break-up, or reduce radiated noise. Most direct numerical simulations (DNS) and large-eddy simulations (LES) have been performed for round or planar jets. Much less computational and experimental data exist for fully three-dimensional nozzle shapes. In this study, a high-order simulation method has been developed for non-axisymmetric jet flows solving the three-dimensional compressible Navier–Stokes equations on a Cartesian domain. The main objectives of this study are (i) to investigate in detail the dynamics of rectangular jets at a sufficiently low Reynolds number at which DNS is feasible, and (ii) to provide reference data for later validation of LES. We point out that a direct comparison of LES results with experiments for this flow configuration is problematic since the experimental inflow conditions—affected, e.g., by nozzle and reservoir geometries—are often not well documented and can thus be matched only approximately in the simulations.

2. Flow Configuration

A rectangular jet configuration was chosen with an aspect ratio of $L_1/L_2 = 5$, a Reynolds number based on the jet center velocity and the height of the nozzle exit L_2 of 2000 and a Mach number of 0.5. The configuration and the coordinate system are illustrated in Fig. 1. We denote the y-axis as the major and the z-axis as the minor jet axis, respectively. The geometry and flow parameters, except for the Reynolds number, were adapted to match the experiments of Tsuchiya et al. (1986). The computational domain measures $37.5L_2 \times 35L_2 \times 35L_2$ (in x, y, z). This is large enough to capture the beginning of the *characteristic-decay* region of the mean velocity at the jet center as defined by Sforza et al. (1966), however, it does not extend into the subsequent *axisymmetric-decay* region.

We do not model the nozzle itself within the domain, but instead use an inflow profile with velocity half-widths corresponding to the nozzle dimensions. For the simulations a laminar smoothed top-hat inflow profile for the streamwise velocity component according to Yu and Monkewitz (1990)

* Corresponding author.
E-mail address: rembold@ifd.mavt.ethz.ch (B. Rembold).

0142-727X/02/$ - see front matter
PII: S0142-727X(02)00150-9

Nomenclature

L_1, L_2	nozzle dimensions
x, y, z	down- and cross-stream coordinate directions
ρ	density
u, v, w	down- and cross-stream velocity components
ξ, η	dimensionless coordinates
B_i, $i = 2, 3$	box dimensions in the lateral directions
Γ_i, k_i, $i = 2, 3$	mapping parameter
n_1, n_2	parameters of the inflow velocity profile
δ	vorticity thickness
$\mathbf{U}$	vector of conservativey variables
$\mathbf{F}(\mathbf{U})$	flux operator
$\sigma(x)$	sponge coefficient
α, β	sponge parameters
$\mathbf{U}_0$	target solution in sponge region
$\theta(\eta)$	blending function
$\hat{u}$	eigenfunction of streamwise velocity
ω	temporal frequency
$\langle\cdot\rangle$	statistically averaged quantity
$\cdot''$	Favre fluctuations
τ_{ij}	Reynolds stresses

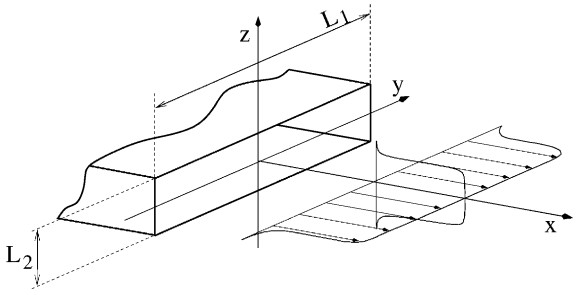

Fig. 1. Jet geometry and coordinate system.

$$u(\eta) = \frac{1}{1 + \sinh(|\eta| \cdot \sinh^{-1}(1))^{2n_i}} \tag{1}$$

was used along both jet centerlines. Here, η is the cross-stream coordinate normalized by the corresponding nozzle half-width $L_i/2$, $(i = 1, 2)$. The parameters $n_1 = 9$ and $n_2 = n_1 L_2/L_1$ are chosen to ensure equal vorticity thicknesses $\delta = \delta_i = L_i/(\sqrt{2} n_i \sinh^{-1}(1))$ in both directions. The cross-stream velocity components of the laminar inflow profile are set to zero.

3. Stability analysis

The transition process of the jet is very sensitive to minor changes of the inflow conditions, since a small variation can lead to an excitation of different instability modes in the laminar jet. By merely enforcing a laminar profile as described above, transition would be triggered mainly by numerical roundoff errors. It is therefore important to impose well defined inflow disturbances. In our simulation we use a spatially developing unstable eigensolution of linear stability theory to initiate transition in a controlled way. Based on the velocity profile (1) and assuming parallel two-dimensional flow we have performed an inviscid spatial linear stability analysis to obtain the most unstable non-oblique spatial modes, which are the sinuous (asymmetric) and varicose (symmetric) mode, respectively. In our simulation we superimpose the varicose mode of the plane jet profile on the laminar inflow profile (see description of boundary conditions below). In Fig. 2 the eigenfunction of the streamwise velocity component is shown for the spatially most amplified varicose mode.

4. Simulation method

4.1. Numerical discretization

The three-dimensional compressible Navier–Stokes in conservation form are solved on a Cartesian grid. For spatial discretization a fifth order compact upwind-biased scheme (Adams and Shariff, 1996) is used for the convective terms and a sixth order compact central scheme (Lele, 1992) for the diffusive terms. Time integration is performed with a third order low-storage Runge–Kutta scheme (Williamson, 1980). We use a Cartesian grid with $337 \times 229 \times 229$ points (in x, y, z) which

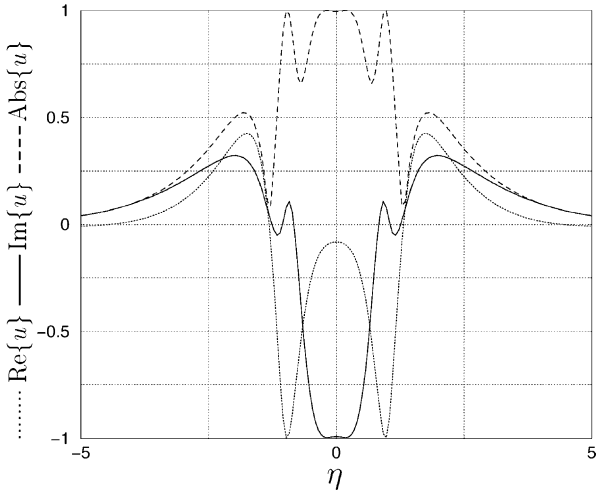

Fig. 2. Eigenfunction of the streamwise velocity component vs. the normalized cross-stream coordinate.

is condensed in the jet center area in the cross-stream direction and equidistant in the downstream direction. The refinement in the cross-stream directions towards the jet center is achieved by a hyperbolic tangent coordinate mapping, which maps the computational domain (ξ_i) onto the physical domain (x_i)

$$\xi_i \in [-0.5, 0.5] \mapsto x_i \in [-B_i/2, B_i/2],$$
$$x_i(\xi_i) = \frac{1}{k_i} \operatorname{artanh}\left(\frac{2\xi}{\Gamma_i}\right), \quad i = 2, 3, \tag{2}$$

where $\Gamma_i = 1/\tanh(k_i B_i/2)$ involves B_i, which is the box dimension in the corresponding cross-stream direction. The parameters k_i were set to 0.46 ($i = 2, 3$). The metric terms are computed analytically from this mapping.

4.2. Boundary conditions

For the simulation of turbulent flow in an open environment the proper formulation of the artificial boundary conditions at the computational-domain boundaries is crucial. On one hand, large vortical structures have to leave the computational domain at the outflow boundary without being unphysically reflected, and on the other hand entrainment has to be allowed in the cross-stream directions. Additionally, acoustic waves originating from the transition region must be allowed to leave the domain without affecting the flow by backward reflection. The accurate and efficient formulation of these artificial boundary conditions for the Navier–Stokes equations in three space dimensions is yet an unsolved problem. However, it is found in practical simulations (e.g. Adams, 1998; Stanley and Sarkar, 1999) that a combination of one-dimensional non-reflecting boundary conditions (Thompson, 1987) and sponge layers, which are added at the far-field boundaries, gives reasonable results. In the sponge layers the governing transport equation for the vector of conservative variables $\mathbf{U}$ is modified according to

$$\frac{\partial \mathbf{U}}{\partial t} = \mathbf{F}(\mathbf{U}) - \sigma(\mathbf{U} - \mathbf{U}_0), \tag{3}$$

where we have written the flux terms of the Navier–Stokes equations briefly as $\mathbf{F}(\mathbf{U})$, so that the solution is driven towards a given steady target solution $\mathbf{U}_0$. The coefficient $\sigma = \sigma(\xi) \geqslant 0$ is non-zero only in the sponge layers and is of the form $\sigma(\xi) = \alpha\xi^\beta$, $0 < \xi < 1$, where ξ denotes a normalized coordinate across the sponge. This numerical algorithm was validated by comparison with linear stability theory. Growth-rate comparisons for unstable eigensolutions of parallel jets have shown a very good agreement with linear theory, where the parameters $\alpha = 2$, $\beta = 3$ were used. The sensitivity of the results to the sponge parameters α and β is weak.

In this simulation the target solution $\mathbf{U}_0$ is chosen to be equal to the quiescent ambient flow, except at the outflow, where it is a two-dimensional Gaussian velocity profile with velocity half-widths estimated from experimental data. The mass flux through the outflow plane is unknown a priori, since ambient fluid is entrained by the jet. For the formulation of an appropriate outflow boundary condition, we approximate the outflow sponge target solution by matching the mass flux through the outflow plane to the influx through the jet at inflow. Entrainment is possible, since the sponge formulation does allow the solution at the outflow to develop. We believe, that this boundary treatment has only a weak influence on the jet transition. At the inflow plane we apply Dirichlet conditions and use an additional sponge layer outside of the jet inflow region to prevent spurious reflections from the inflow boundary. The inflow mean profile is chosen according to Eq. (1) along the two axes of the jet. Along the center of the rectangular inflow profile ($|y| < L_1/2$) we assume the flow to be mainly two-dimensional and therefore superimpose the eigenfunction of the spatially most unstable varicose mode for the two-dimensional velocity profile computed from linear stability theory (see above). At the edges and outside of the nozzle region ($|y| \geqslant L_1/2$) we smoothly ramp the superimposed eigenfunction to zero by multiplication with

$$\theta(\eta) = \exp\{-(1.2\eta)^8\}. \tag{4}$$

Here again η is equal to the y-coordinate normalized with the nozzle half-width $L_1/2$. We enforce an amplitude of the inflow disturbance such that $\max(\hat{u})/\max(u) = 0.005$ at $x \approx L_1$, where $\hat{u}$ denotes the amplitude of the eigenfunction of the streamwise velocity variable u. The frequency ω predicted by linear stability theory, and confirmed by DNS, is 2.7066 (normalized with $L_1/2$ and the jet center velocity at the inflow).

5. Results

The simulation was started using the undisturbed laminar inflow profile throughout the entire computational domain on a coarse grid. After an initial transient the grid was refined to the actual grid by high order spline interpolation. Sampling was started after a second transient due to the interpolation had faded. A total of 1200 samples from a dimensionless time interval of about 470 (207 periods of the harmonic excitation) spanned by roughly 3.3×10^5 timesteps was analyzed. Note that because of the three-dimensionality of the flow no homogenous direction can be exploited for additional averaging to improve statistical data. However, sector symmetry over the four quadrants of the rectangular profile can be exploited. In the following we first present instantaneous flow data to visualize the flow topology and second we show time- and sector-averaged data.

5.1. Instantaneous data

In Fig. 3 the instantaneous flow topology of the transition process is visualized by a density iso-surface. We observe a strong growth of the linear instability mode in the laminar region. Rapidly three-dimensional disturbances of the initially two-dimensional instability mode grow at the lateral edges of the jet. A symmetric vortex structure develops but breaks up almost immediately into small-scale turbulence. To visualize this transitional vortical structure, we show in Fig. 4 a close-up of a pressure iso-surface in the transition region. Vortices symmetric to the (x, y)-plane can be identified which deform and finally break up into disordered structures. Additionally, Fig. 5 displays density plots in two cross-sections through the jet center. The excited varicose mode develops towards the antisymmetric sinuous mode which is followed by a rapid transition to turbulence. The observed flow structure and transition location are the result of the imposed inflow disturbances. Since the most unstable eigenmode would also develop naturally, a similar transition topology and location would be obtained using a broad-banded disturbance spectrum and adapting the amplitude levels.

Fig. 3. Snapshot of density iso-surface.

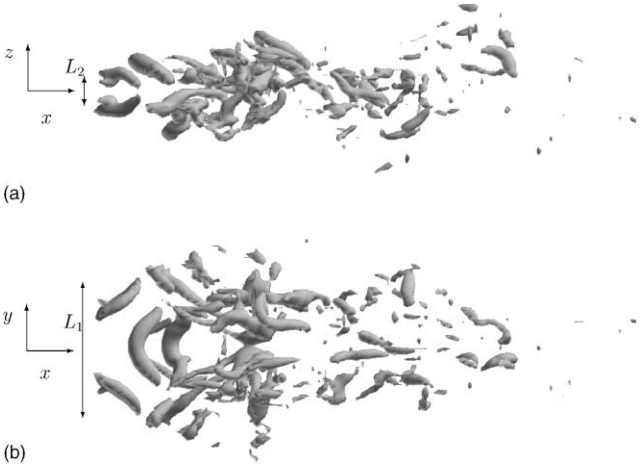

Fig. 4. Snapshot of pressure iso-surface in the transition region. Side view (a) and top view (b), flow from left to right.

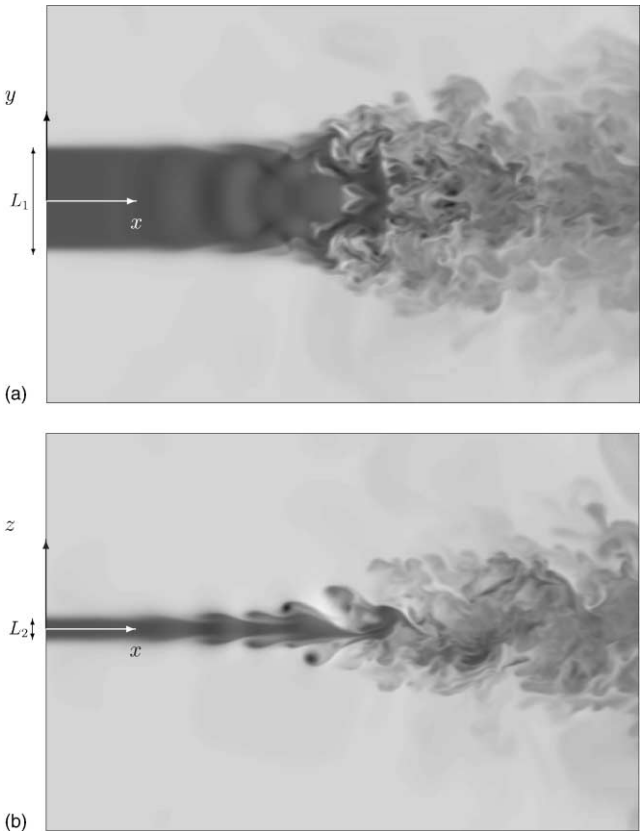

Fig. 5. Snapshot of density contours along the major (a) and minor (b) axis of the jet at the same instant.

However, small-scale contributions of random noise render the perturbations grid dependent, which is undesirable and gives rise to systematic differences between LES and DNS.

5.2. Statistically averaged data

To assess the mean properties of the analyzed flow we show sector- and time-averaged flow data at nine equidistantly spaced downstream stations (each 36th grid plane, which corresponds to a distance between the stations of 4.02 L_2) where the first station represents the inflow plane. We plot the data along the major and the minor axes of the jet. Note that the last station is still well before the beginning of the sponge zone at the end of the computational domain. We use the notation $\langle\,\rangle$ for sector- and time-averaged variables.

In Fig. 6(a) and (b) the streamwise velocity profiles $\langle u \rangle$ are shown. Ahead of the transition region the jet profile spreads only marginally due to diffusion. After transition has taken place, one observes a strong spreading of the profiles away from the major axis, so that the entire profile transforms towards an elliptical shape. In the transition region itself a non-monotonic profile is

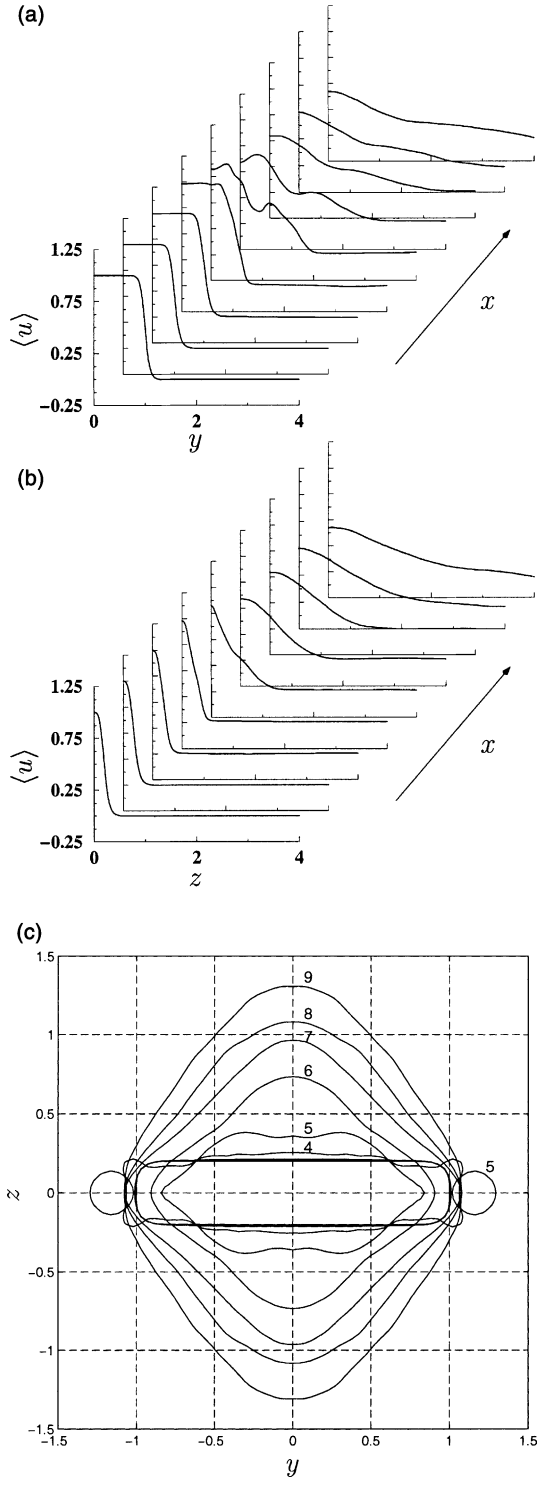

Fig. 6. Mean streamwise velocity profiles $\langle u \rangle$ at different downstream stations; along major (a) and minor (b) axis. (c) Downstream development of the velocity half-width contours $\langle u \rangle(x, y, z) = 1/2\langle u \rangle(x, 0, 0)$ at the same downstream stations as Figs. 6–10. Station 4–9 are labeled for clarity.

observed, which is caused by correlated large scale structures present in this region. In Fig. 6(c) we plot downstream velocity half-width contours $\langle u \rangle(x, y, z) = 1/2\langle u \rangle(x, 0, 0)$ at the nine downstream stations. The different spreading behavior of the jet with respect to its two symmetry axes can clearly be identified. Whereas a strong expansion of the jet along its minor axis takes place immediately, even a slight contraction is observed along its major axis. Only towards the end of the computational domain the velocity half width of the inflow profile is recovered. Qualitatively this corresponds to experimental observations (Tsuchiya et al., 1986). From the same experiments for non-axisymmetric jets it is also known that in the transition region a so-called *saddle-back* profile occurs along the major axis of the mean flow. Here, the mean centerline streamwise velocity drops below the value reached in the surrounding shear layers. Our simulation is qualitatively in good agreement with these findings, see Fig. 6(a), fifth and sixth station. In Fig. 7 the transverse velocity components $\langle v \rangle$ and $\langle w \rangle$

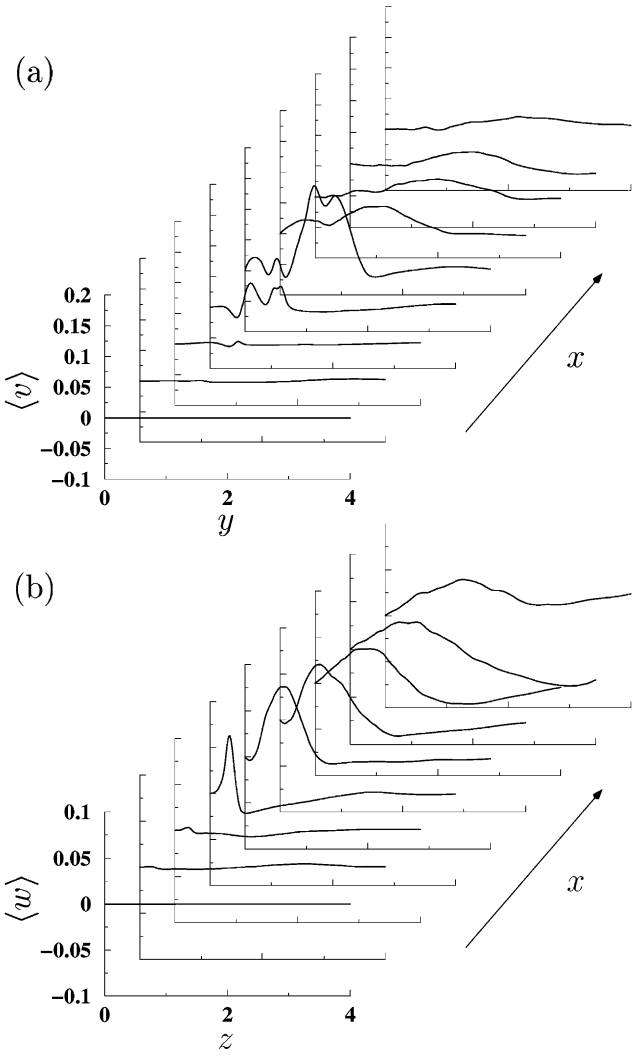

Fig. 7. Mean cross-stream velocity profiles at different downstream stations; $\langle v \rangle$ along major (a) and $\langle w \rangle$ along minor (b) axis.

are plotted. The averaged velocity components in the direction orthogonal to the jet center planes vanish due to symmetry and are not shown. In the transition region one observes a peak of the cross-stream velocity components, which is roughly twice as high along the major axis as along the minor axis whereas in the turbulent regime the profiles flatten out again.

For an investigation of turbulent statistics we examine the development of the turbulent kinetic energy k defined by $\langle \rho u_i'' u_i'' \rangle / 2$, the Reynolds normal stress $\tau_{11} = \langle \rho u'' u'' \rangle$ and the Reynolds shear stresses $\tau_{12} = \langle \rho u'' v'' \rangle$ and $\tau_{13} = \langle \rho u'' w'' \rangle$. The number of samples computed is obviously not sufficient to obtain smooth profiles especially in the developed turbulent regime. The roughness of the profiles in the transition region, however, is believed to be caused by the deterministic inflow forcing used in this simulation. It is evident and was also repeatedly shown in experiments, that the turbulence levels increase rapidly when the jet undergoes transition. However, this process probably depends strongly on parameters such as the shape of the nozzle, initial turbulence intensity, Reynolds number, etc. This makes it difficult to compare computational and experimental data, since experimental inflow and lateral conditions are usually not known with sufficient accuracy. In this simulation we find a rapid growth of the Reynolds stresses beginning roughly at a distance of $13L_2$ downstream of the nozzle (see Figs. 8 and 9). They reach peak values at the jet edges along the major axis, from where three-dimensional disturbances of the transition process originate. The same holds for the turbulent kinetic energy which is plotted in Fig. 10.

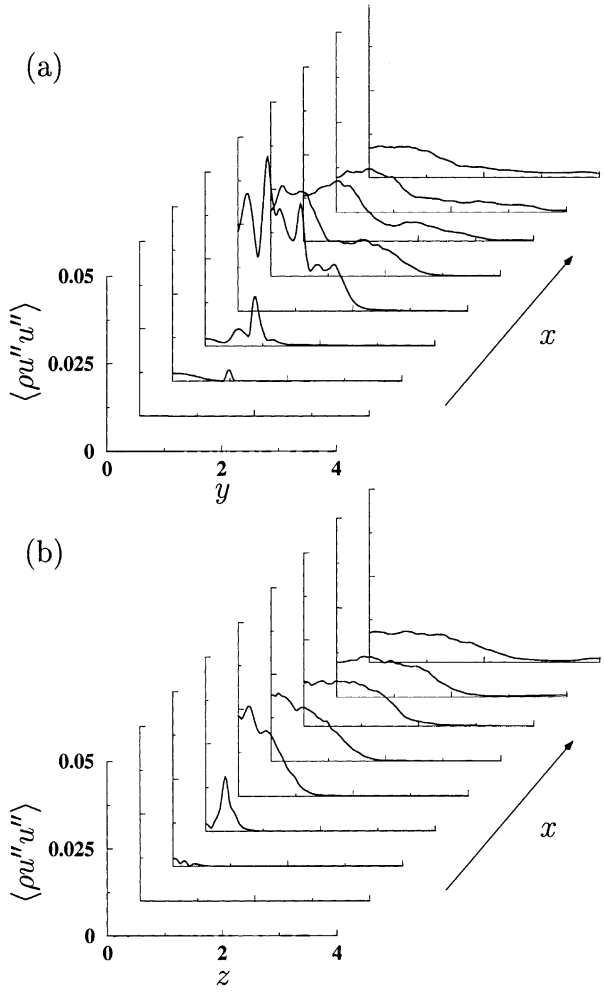

Fig. 8. Reynolds normal stress $\langle \rho u'' u'' \rangle$ at different downstream stations; along major (a) and minor (b) axis.

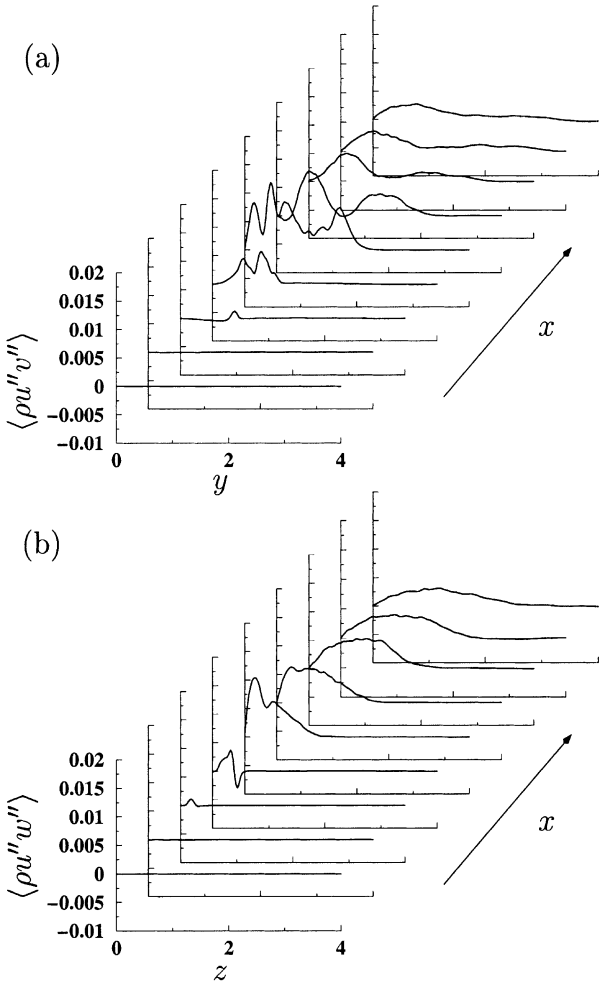

Fig. 9. Reynolds shear stresses at different downstream stations; $\langle \rho u'' v'' \rangle$ along major (a) and $\langle \rho u'' w'' \rangle$ along minor (b) axis.

6. Concluding remarks

We have presented instantaneous and statistically averaged results of a DNS of a rectangular compressible jet configuration which was performed in order to investigate the transition process of non-axisymmetric jets

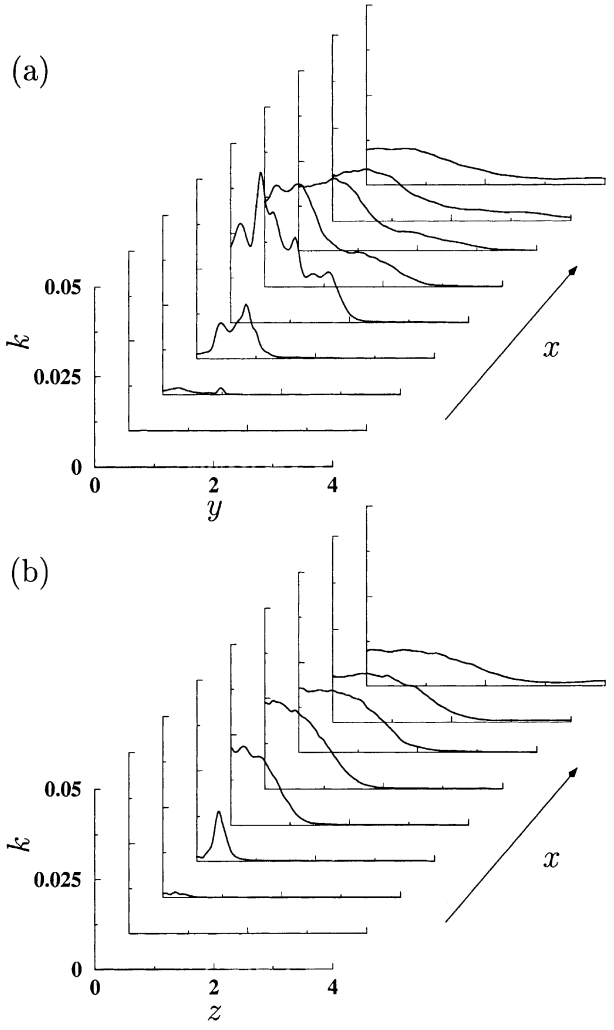

Fig. 10. Turbulent kinetic energy k at different downstream stations; along major (a) and minor (b) axis.

and to provide reference data for future LES. We have imposed well-defined inflow conditions in order to make validation of LES models possible. The transition process shows how the initially two-dimensional disturbances in the inflow region of the jet rapidly grow three-dimensional, which leads to a breakdown of the jet to small-scale turbulence. The non-axisymmetry of the profile causes a strong spreading of the jet along its minor axis, which is consistent with experimental findings.

Acknowledgements

This work was supported by the Swiss National Science Foundation. Computations have been performed at the Swiss Center for Scientific Computing in Manno (CSCS).

References

Adams, N.A., 1998. Direct numerical simulation of turbulent compression corner flow. Theor. Comp. Fluid Dyn. 12, 109–129.

Adams, N.A., Shariff, K., 1996. A high resolution hybrid compact-ENO scheme for shock-turbulence interaction problems. J. Comput. Phys. 127, 27–51.

Gutmark, E.J., Grinstein, F.F., 1999. Flow control with noncircular jets. Ann. Rev. Fluid Mech. 31, 239–272.

Lele, S.K., 1992. Compact finite difference schemes with spectral-like resolution. J. Comput. Phys. 103, 16–42.

Sforza, P.M., Steiger, M.H., Trentacoste, N., 1966. Studies on three-dimensional viscous jets. AIAA J. 4 (5), 800–805.

Stanley, S.A., Sarkar, S., 1999. Direct numerical simulation of the developing region of turbulent planar jets. In: 37th AIAA Aerospace Sciences Meeting and Exhibit no. 99-0288. AIAA, Reno, Nevada.

Thompson, K.W., 1987. Time dependent boundary conditions for hyperbolic systems. J. Comput. Phys. 68 (1), 1–24.

Tsuchiya, Y., Horikoshi, C., Sato, T., 1986. On the spread of rectangular jets. Exp. Fluids 4, 197–204.

Williamson, J.H., 1980. Low-storage Runge–Kutta schemes. J. Comput. Phys. 35, 48–56.

Yu, M.H., Monkewitz, P.A., 1990. The effect on nonuniform density on the absolute instability of two-dimensional inertial jets and wakes. Phys. Fluids A 2 (7), 1175–1181.